JOURNAL OF MATERIALS SCIENCE 19 (1984) 2121–2135

Electron emission measurements and the defect structure of α-Al_2O_3

P. ODIER, J. C. RIFFLET
Centre de Recherche sur la Physique des Hautes Températures, Centre National de la Recherche Scientifique, 1D Avenue de la Recherche Scientifique, 45045 Orleans, Cedex, France

J. P. LOUP
Laboratoire de Physique Electronique et Thermodynamique des Oxydes, Faculté des Sciences, Parc de Grandmont, 37200 Tours, France

In this article, electron emission is used to study the defect structure of α alumina. The need of a direct measurement of the position of the Fermi level (or the electron concentration in the conduction band) is shown by discussing the actual electrical data on alumina. The emission has been measured over a large temperature range (1400 to 2400 K) and the emission of a technical polycrystalline alumina is reported up to the melting temperature under a controlled oxygen partial pressure. Additional results are reported for titanium- and iron-doped polycrystalline aluminas. The results are discussed from two points of view. First the quantitative data concerning the work function are taken into account and the contribution of the surface layer is discussed. Secondly, the dependency of the electron emission on the oxygen partial pressure is explained by the defect chemistry of the oxide. The absence of variation of the electron concentration in a certain range of P_{O_2} is due to a self compensation between donor and acceptor impurities.

1. Introduction

In the last decade extensive work on the defect structure of α-Al_2O_3 at high temperature has been undertaken mainly by Kröger and co-workers; some significant publications of this group are cited [1–10] and will be used in the following pages. In such studies the authors use combined measurements of electrical conductivity and transference numbers associated with optical and magnetic determinations of the dopant concentration.

It is now agreed that the intrinsic concentration of ionic defects at stoichiometry is extremely small (in the range 10^8 cm^{-3} at 1900 K according to Mohapatra *et al.* [7], compared to 10^{17} cm^{-3} for TiO_2 at the same temperature [11]) and one of the most severe problems encountered in interpreting experimental data is the influence of impurities.

In defect structure studies, the electrical conductivity is widely used as a convenient method, although several parameters are generally unknown such as the mobility of the carriers and the state of ionization of donors or acceptors which is determined by the position of the Fermi level in the forbidden gap. Electron emission is very sensitive to the position of the Fermi level in the gap as a result of the exponential law controlling the emission of electrons. At a first approximation:

$$J_0 = A_0 T^2 \exp -\frac{E_{vac} - E_F}{kT} \quad (1)$$

where J_0 is the emitted current density (A m^{-2}), A_0 is a constant, T the absolute temperature, E_{vac} the electron energy in the vacuum and $E_{vac} - E_F$ represents the work function [12]. In Equation 1 a mean reflection coefficient at the barrier has been neglected.

The present authors use this method for study-

0022–2461/84 $03.00 + .12

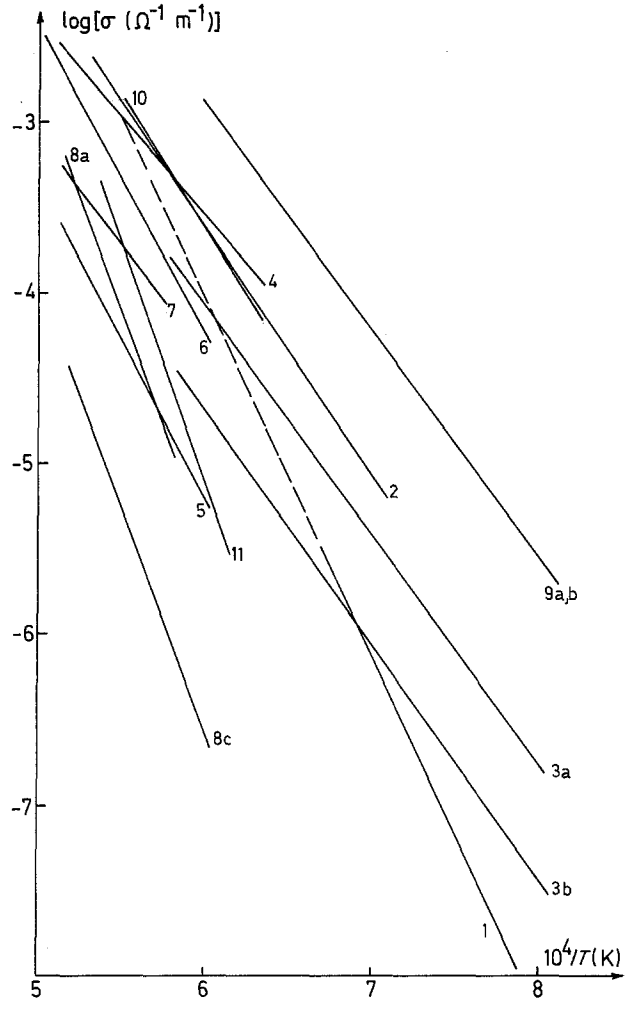

Figure 1 Electrical conductivity data reported for single crystals of α-Al_2O_3. Measurements made in air, the main impurities of the sample were, respectively: 1 [18]: Na, Si, Ca; 2 [3]: Si, Co; 3(a) sample IV of [1]: Mg, Fe, Si; 3(b) sample V of [1]: Ti, Si, Ca; 4 same as 3(a) [5]; 5 [6]: Ti, Si, Ca; 6 [19]: Si, Co; 7 sample I of [8]: Si, Mo, Ca; 8(a) sample II of [8]: Si, Na, Fe; 8(b) sample II_a of [8]: Si, Na, Fe; 9 sample 3 of [21]: Fe, Si, B, Ca; 10 [4, 15]: Fe, Si; 11 [20]: Si, Co, Bi.

ing the defect structure of pure oxide at high temperature [13, 14] and consider that it provides new information in the case of α-Al_2O_3.

After a short survey of the defect chemistry of alumina, experimental results on electron emission are reported for technical alumina and alumina doped with titanium and iron. The experiments were performed between 1400 and 2400 K under controlled oxygen pressures. The results are discussed in terms of native point defects and impurities.

2. The electrical properties of alumina at high temperature

It is appropriate to distinguish between single crystal and polycrystalline material, which behave differently as a consequence of grain boundaries. Single crystal properties will be examined first.

2.1. Single crystal

Since the publication of the paper of Papis and Kingery [15] in 1961 there have been many improvements in the technique of measuring high-temperature conductivity. A significant step was made in 1964 when Loup and co-workers [16, 17] recognized that surface conduction or gas leakage at high temperature is important in investigations on low conductivity materials. The mostly frequently used technique is a three-point measurement with a guard ring and grounded tubes to collect the charges present in the gas phase at high temperature (> 1800 K) [12, 18–20]. An alternative method consists in using a sample in the shape of a tube long enough to neglect surface conduction [20, 21]. Most pertinent publications on single crystals, made by the three-point or tube technique, are replotted in Fig. 1. A large discrepancy remains between the various investigations: an order of magnitude for a mean value of 3.0×10^{-3} $(\Omega\,m)^{-1}$ at 1900 K in air. One reason for such a spread is the poorly controlled purity of the samples. According to chemical analysis,

TABLE I Incorporation reactions for a donor or an acceptor in α-Al_2O_3

Donor D		Acceptor A
I low P_{O_2}	$2DO_2 \rightarrow 2D^{\cdot}_{Al} + 3O^{x}_{O} + \frac{1}{2}O_2 + 2e'$	III $2AO \rightarrow 2A'_{Al} + V^{2\cdot}_{O} + 2O^{x}_{O}$
II high P_{O_2}	$2DO_2 \rightarrow 2D^{\cdot}_{Al} + 3O^{x}_{O} + O^{2'}_{i}$ $3DO_2 \rightarrow 3D^{\cdot}_{Al} + V^{3'}_{Al} + 6O^{x}_{O}$	IV $2AO + \frac{1}{2}O_2 \rightarrow 2A'_{Al} + 2h^{+} + 3O^{x}_{O}$
V	$\frac{3}{2}O_2 \rightleftarrows 2V^{3'}_{Al} + 3O^{x}_{O} + 6h^{+}$ $\frac{1}{2}O_2 \rightleftarrows O^{2'}_{i} + 2h^{+}$	VI $O^{x}_{O} \rightleftarrows \frac{1}{2}O_2 + V^{2\cdot}_{O} + 2e'$
VII	$D^{x} \rightleftarrows D^{\cdot} + e'$	VIII $A^{x} \rightleftarrows A'_{Al} + h^{+}$
	$np = k_i$	

Neutrality: $3[V^{3'}_{Al}] + 2[O^{2'}_{i}] + n + [A'] = p + [D^{\cdot}] + 2[V^{2\cdot}_{O}]$ (3)

even for the doped samples, there is generally more than one impurity which should be taken into account. Careful observation, however, leads to the following conclusions: a high conductivity occurs when magnesium, cobalt and iron ions are present whereas titanium and sodium apparently lower it. The effect of silicon is not clear as it is detected as a significant impurity in all these samples. The contribution of the impurities to the electrical conductivity can be understood through the defect chemistry of the oxide.

An important step has been to show that the conductivity of alumina doped with acceptors (magnesium, cobalt, iron) is essentially different from that of crystals doped with a donor (titanium): transference number measurements [1–10] show that in air the former are p-type electron conductors while the latter are ionic conductors. At low oxygen partial pressure the reverse is observed and this emphasizes the part played by the equilibrium between the gas phase and the solid. These observations are explained qualitatively by the reaction given in Table I, in which the Kröger–Vink notation is used [22]. When oxygen is present in the gas phase, donor impurities will be incorporated within the lattice preferentially through Reaction II involving aluminium vacancies or interstitial oxygens, as a consequence the ionic conduction is likely to be observed. At low P_{O_2} for donor impurities (high P_{O_2} for acceptors) the electron (or hole) conductivity become dominant because impurities are incorporated according to Reaction I or IV involving electrons and holes whose mobilities are higher than that of ions.

For a quantitative analysis, the concentration of defects must be calculated using the equations given in Table I. In order to manipulate the analytical expressions, one must assume, for example, that $[A^{x}_{Al}] \ll [A'_{Al}]$ or $[A'_{Al}] \ll [A^{x}_{Al}]$ or have a knowledge of the degree of ionization ($[A'_{Al}]/[A^{x}_{Al}]$). This is controlled by the position of the Fermi level according to Fermi–Dirac statistics [23]:

$$\frac{[A'_{Al}]}{[A^{x}_{Al}]} = \frac{g_1}{g_2} \exp \frac{E_F - E_A}{kT} \qquad (2)$$

where g_1 and g_2 are the statistical weights of the species and E_A the energy of the level A (E_A is referred to the valence band). A similar equation may be written for donor states. The pre-exponential factor entering Equation 2 has the value 12 for cobalt, 2.5 for iron and 8.0×10^{-2} for magnesium [10]. In the case of doping by cobalt, one can consider that $[Co'_{Al}] \gg [Co^{x}_{Al}]$ when $E_F \simeq E_{Co}$, but a similar inequality occurs for magnesium doping only when $E_F - E_{Mg} \simeq 5\,kT$ corresponding to E_F located 0.8 eV above E_{Mg} at 1900 K; the case of iron is in between these two cases. If donor impurities are present in addition to the acceptor dopant, the Fermi level is raised somewhere between the two levels and the ionization of the acceptor will be significantly higher. Such a process is expected in the magnesium-doped crystal used in [5]. If one takes account of donor impurities (presumably silicon or sodium), the concentration $[Mg'_{Al}]$ calculated from the conductivity data is significantly higher than when donor impurities are neglected as was assumed in [5]. Thus the degree of ionization is probably larger than expected by the authors.

Another essential parameter in the quantitative analysis of the electrical data is the energy of the level E_A. Kröger *et al.* [1–10] have attempted to evaluate it by a rather indirect method from data obtained by electrical conductivity measured under non-equilibrium conditions. The main assumptions of their calculation are:

1. $[A'_{Al}]/[A^{x}_{Al}]$ is constant and there is no

TABLE II Energy levels in α-Al_2O_3 (eV); energy gap $E_g = 10 - 1.5 \times 10^{-3}\ T^{2.9}$, electron affinity χ (300 K) $\simeq$ 1 eV[11]

Acceptors $E_A - E_V = (E_A - E_V)^0 - \beta T$			Donors $E_C - E_D = (E_D - E_V)^0 - \beta T$			
	300 K	1900 K			300 K	1900 K
Mg thermal	1.83[1]	1.19[1] $\beta \simeq 4\ 10^{-4}$ eV K^{-1}	Ti	thermal	2.4[9]	2.01[10] $\beta \simeq 4\ 10^{-4}$ eV K^{-1} 2.76[2]
				optical	3.8[9] 4.25[10]	
Co thermal		3.06[2,3]				
optical	4.0[4,5]					
Fe thermal		2.97[6] $\beta \simeq 5\ 10^{-4}$ eV K^{-1} 4.73[2]				
optical	4.8[7]					
A thermal		2.35[8]	D	thermal		3.17[8] $\beta \simeq 5\ 10^{-4}$ eV K^{-1}
A* thermal		3.47[8] $\beta \simeq 5\ 10^{-4}$ eV K^{-1}	D*(H)	thermal		4.17[3] 5.92[2]

A, A*, D and D* are non-identified acceptors and donors
[1] [5]; [2] [10]; [3] [3]; [4] [44]; [5] [45]; [6] [4]; [7] [46–49]; [8] [8]; [9] [43]; [10] [6]; [11] [25, 26].

charge redistribution on traps levels during the experiment;

2. the values of the mobility and the variations of the energy levels with the temperature are known.

Even with such assumptions the attempt is very interesting as it gives an order of magnitude for the thermal energy values which may be different from optical ones [24]. Table II [3–6, 8, 10, 25–27, 43] summarizes the values extracted by Kröger *et al.* for several dopants as compared with other determinations; indicated also is the thermal band gap and the electron affinity ($E_{vac} - E_C$). This last quantity is small compared to that of other oxides [27] and its variation with temperature is unknown. All these values are plotted together in Fig. 2 assuming a negligible variation of χ with T.

In order to have a complete analysis of a compound it is generally necessary to simplify the neutrality equation: Equation (13) in Table I. One often makes the assumption that a dopant predominates among various impurities and this allows one to neglect certain defects. For example in titanium-doped crystals, $V_{Al}^{3'}$ or $O_i^{2'}$ are supposed to predominate [6] with $V_{Al}^{3'}$ being the most likely species; in crystals doped with acceptors (magnesium, cobalt, iron), $Al_i^{3\cdot}$ or $V_0^{2\cdot}$ will probably be

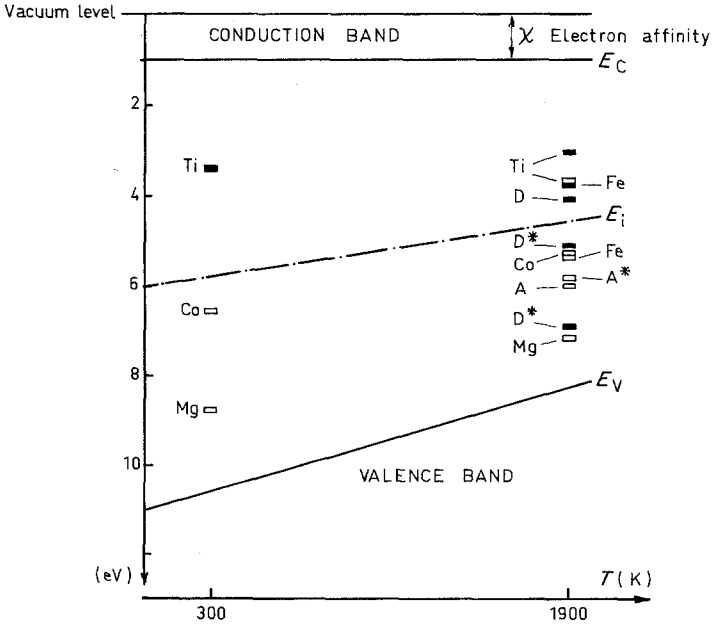

Figure 2 Energy diagram in Al_2O_3 according to Table II. For simplicity the electron affinity χ is assumed to be independent of T.

in a majority [3–5]. This is, however, only a rough assumption in compounds where impurities are often in the same order of concentration as the dopant; the compensating impurities are expected to reduce the effect of the dopant on the electrical conductivity. This is probably why there is only a small difference (less than a factor two) between the hole conductivities of magnesium-, cobalt- and iron-doped aluminas.

One can conclude this discussion by emphasizing the need for direct measurement of the position of the Fermi level in alumina. The thermo-electric power is useful only for electronic conductors. For mixed conductors it appears to us that thermo-electronic emission measurement is a valuable method, being direct and easy. The experimental method is described in Section 3.

2.2. Polycrystalline solids

A polycrystalline compound is an inhomogeneous material in which the grain boundaries have a structure and a composition which may differ from the bulk. This is obvious when a second phase has precipitated [28] but segregation can also occur without precipitation as in the case of CaO-doped Al_2O_3 [29]. The grain boundaries have an effect on such properties as electrical conductivity [9, 30], chemical diffusion [31], redox kinetics [32], sintering [33] etc. Grain-boundary effects are enhanced by small crystallite diameters and Kröger *et al.* have recently shown their influence on the electronic conductivity of iron- and titanium-doped Al_2O_3 [9, 30, 34] by using samples with controlled grain size. The electronic conductivity rises when the grain size decreases but no such effect is observed on the ionic conduction. A model based on the evaluation of the space charge due to grain-boundary segregation and its effect on the electronic conductivity [30] fits rather well the electronic part: the rise in conductivity can be accounted for by a curvature of the energy bands near the surface due to the segregation of the dopant at the surface of the grains. The absence of variation in the ionic conductivity is not well explained. When the grain size is larger than 10 μm the effect of grain boundaries on the conductivity is negligible [30].

2.3. Conclusions

Summarizing:

1. the electrical properties of alumina at high temperature are controlled mostly by impurities, the concentration of which is generally larger than that of defects formed by native disorder or non-stoichiometry. Acceptors increase the hole conductivity to a value higher than the ionic conductivity in air. On the other hand, donor-doped materials are principally ionic in air. The energy levels of the dopant are not precisely known;

2. the properties of polycrystalline aluminas are controlled by grain boundaries when the grain size is smaller than 10 μm. The properties of these grain boundaries are not well described;

3. measurements of the position of the Fermi level are needed at high temperature and under conditions of controlled oxygen partial pressure.

A method for such measurements using electronic thermo-emission will now be described.

3. Experimental method

The experimental method described here consists mainly in measuring the current of electrons emitted from an oxide heated under a reduced pressure. The oxygen partial pressure is varied by leaking pure oxygen into the vacuum chamber in such a way that the total pressure is adjusted between 10^{-6} and 10 Pa (the atmosphere, monitored by a mass spectometer, is pure oxygen). Heating of the sample is achieved by two methods each being used in a selected temperature range. They both give the same value for the emitted current at identical temperatures.

For temperatures lower than 1900 K an iridium ribbon, directly heated by the Joule effect, is used. The oxide is deposited on one face of the ribbon by a drop (a few mm^3) of a fine powder in suspension in isopropyl alcohol. After slow drying, a smooth layer of 10 to 50 μm is obtained which is then sintered in air at 1500 K. The layer is mechanically resistant and sticks well to the metal. The small thickness ensures that its temperature is the same as that of the metal support, particularly at high temperature where most of the heat transfer is made by radiation. The temperature is measured by optical pyrometry on the back face of the ribbon. Since very high temperature experiments may change the surface morphology by grain growth, the sample is initially heated at high temperature (1900 K) under 10^{-1} Pa oxygen in order to stabilize the surface morphology. After this procedure the experiments are reproducible. The emitted current of electrons is measured by the diode technique with two circular concentric

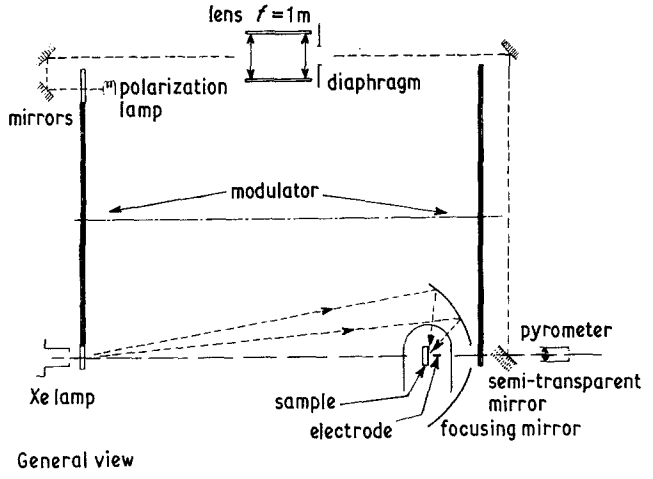

Figure 3 Experimental apparatus for the high-temperature experiment.

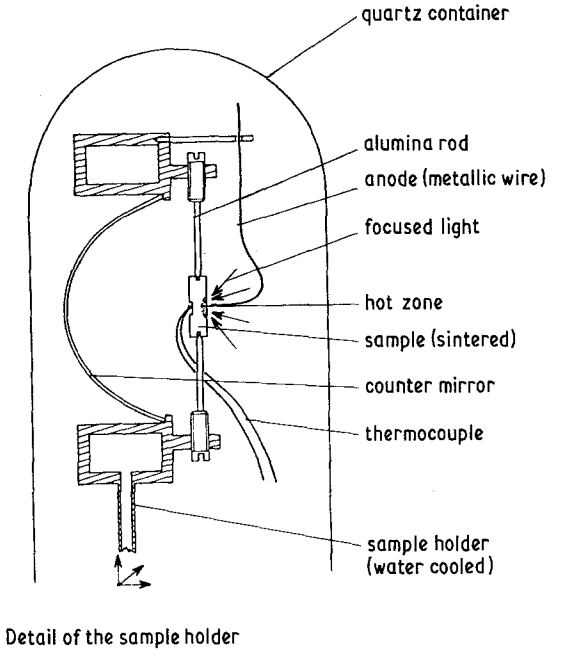

electrodes. The central anode has a surface smaller than the oxide layer so that the emitting area is known (10 to 20 mm^2) and the outer one acts as a guard, defining parallel lines for the electric field. The Schottky law is used to extrapolate the current to zero field [27].

For temperatures higher than 1900 K, an image furnace is used to heat the sample. The light of a high-pressure xenon lamp is focused on a sintered sample placed at the focal point of an elliptical mirror (Fig. 3). The sample is inside a quartz container connected to a vacuum system having a high pumping speed. Even at very high temperature (3100 K can be reached) the residual pressure is in the range of 10^{-4} Pa. The temperature is measured by optical pyrometry using two pyrometers: one is bichromatic and the other monochromatic. The first is necessary to suppress the problems of optical transmission through the quartz, the second is used for calibration at the melting point of alumina (IUPAC data are used: $T_m(Al_2O_3) = 2327 \pm 6$ K). A special design is used for the electrodes: the cathode is the sample itself, it is electrical connected to the power supply by an iridium wire located at the rear; the anode is a guarded wire facing the sample. Such a configuration is necessary to avoid a shadow of the electrode on the sample. A modulator is also used to

TABLE III Spectrographic analysis (ppm)

Al_2O_3 Degussa (99.7%)			Al_2O_3-Ti (before)	Al_2O_3-Ti (after)
Acceptors	Zn	70	–	–
	Ni	80	30	30
	Mg	1800	180	60
	Fe	800	50	50
	Ca	1000	–	–
	Co	–	50	50
Donors	Si	85	200	350
	Na	200	–	–
	K	60	–	–
	Ti	30	3600	200
	Zr	30	–	–
?	Mn	25	–	–
	Cr	75	–	–
	As	50	–	–

mask the light source when the measurement of the temperature is made. The $I-V$ curve of the diode is obtained using a sawtooth voltage waveform synchronous with the temperature measurement. The emitting area is estimated from a photograph of the hot sample and the current density is determined by dividing the measured current by the estimated area. Temperature non-uniformity across the sample has little effect on the measurement because the low temperature area contributes weakly to the total current as a consequence of the Arrhenius dependence of Equation 1. This method enables us to operate with a satisfying accuracy at very high temperature: the electron emission of alumina has been measured for the first time at the melting point on sintered samples.

Experiments were made on technical alumina (Degussa of 99.7% purity). The main impurities are listed in Table III. Powders of titanium- and iron-doped Al_2O_3 were prepared by Kröger *et al.* and were melted in air by us under a CO_2 laser beam to improve the diffusion of the dopant inside the bulk. After such treatment the powders were respectively, light blue and dark yellow as usual for these dopants. For the titanium-doped material additional weak lines appeared in the X-ray spectrum corresponding to Al_2TiO_5 precipitates.

4. Experimental results

4.1. Technical alumina

Samples of sintered rods (98% theoretical density) were cut and positioned in the arc image furnace (diameter 7 mm, thickness 3 mm). After heating the sample in air up to the melting point, its colour changed from yellow–pink to red–pink. On the other hand, heating in reduced oxygen partial pressure ($P_{O_2} \simeq 10^2$ Pa) turned the initial colour to white. These variations in the colour are apparently due to oxidation–reduction changes of the aliovalent impurities: see Table I. The density of current emitted by the high-temperature method is in good agreement with previous determinations made by the ribbon technique at lower temperature [27]. The results are plotted against oxygen partial pressure in Fig. 4a. There is no variation of the current with oxygen partial pressure in this range P_{O_2}: this is a remarkable property previously unobserved on equilibrated oxides in electron emission studies. A plot of the current against the inverse of the temperature is shown in Fig. 4b. As no dependence on P_{O_2} was observed, its values are not mentioned on the curve. The dotted line corresponds to measurements in the liquid phase. Over this range of temperature the emission is smaller (six times) than expected from an extrapolation of the solid state. This is equivalent to an increase of 160 meV of the work function occurring presumably on melting. For solid samples, the activation energy is around 6 eV.

4.2. Titanium-doped alumina

The experiments were made by the heated ribbon technique. The emission was measured against temperature (Fig. 5a). The activation energy obtained from a plot $\log J_0 - 1/T$ is between 5.9 and 5.5 eV, a value not very different from the value obtained on the technical alumina. Measurements were also made at constant temperature and for decreasing oxygen partial pressure, the sample being re-equilibrated afterwards at high P_{O_2}. Several isotherms were made at increasing temperatures (Fig. 5b). Two samples were investigated, the first of which was not pretreated at high temperature as described in Section 3, the results being, however, essentially identical.

A spectrographic chemical analysis was made before and after the experiment: see Table III. The starting product had 7000 ppm titanium; after pretreatment 3600 ppm was found and only 200 ppm after the experiment. The quantitative analysis is however, subject to caution because of the very small amount of material used in the experiment (few mg). Nevertheless there is a strong indication that some titanium is lost during the experiment. The variation in the magnesium content (Table III) is not significant. Thus the doping concentration is

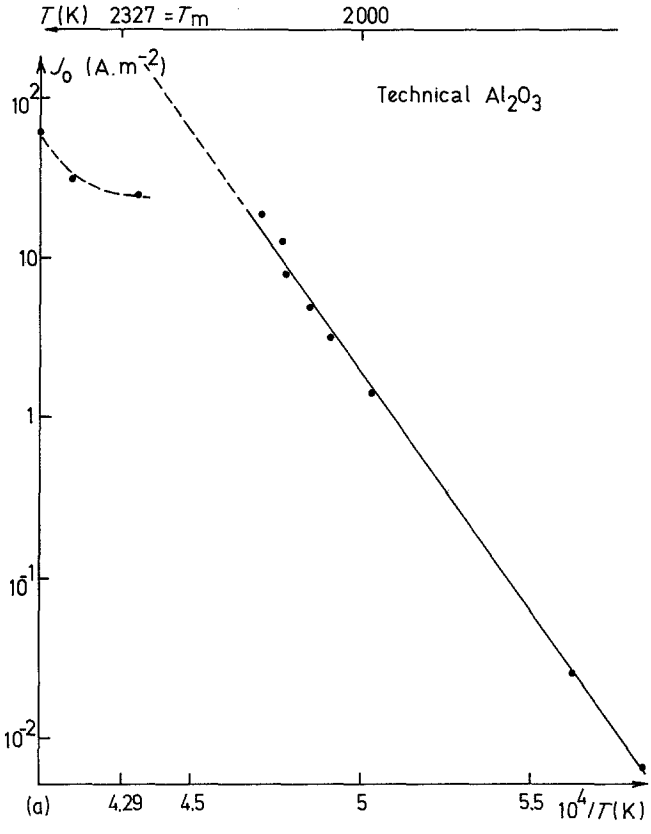

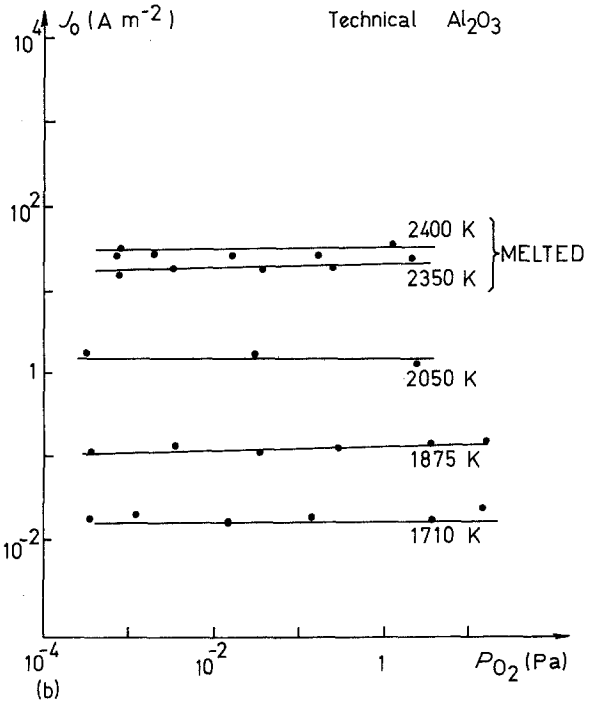

Figure 4 (a) Electron emission of a polycrystalline technical alumina (99.7% pure) as a function of the oxygen partial pressure, P_{O_2}. (b) Electron emission of a polycrystalline technical alumina (99.7% pure) as a function of temperature: the activation energy is $\simeq 6$ eV.

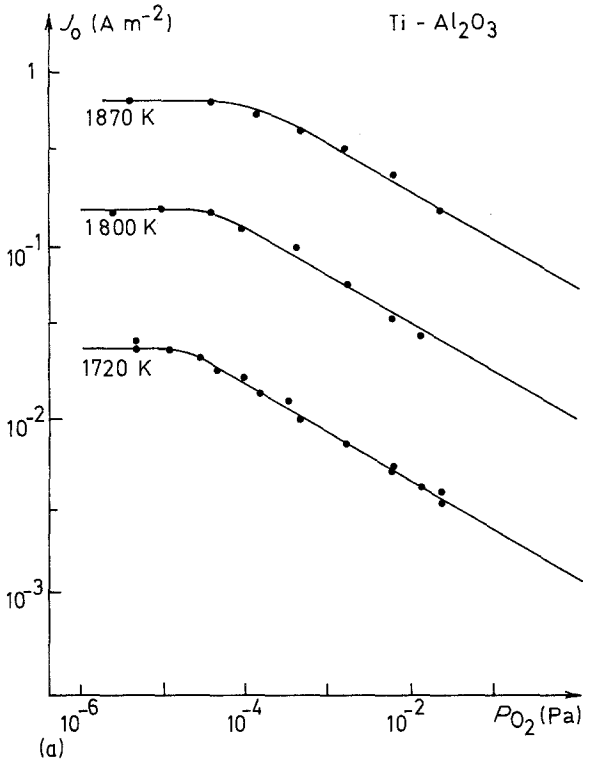

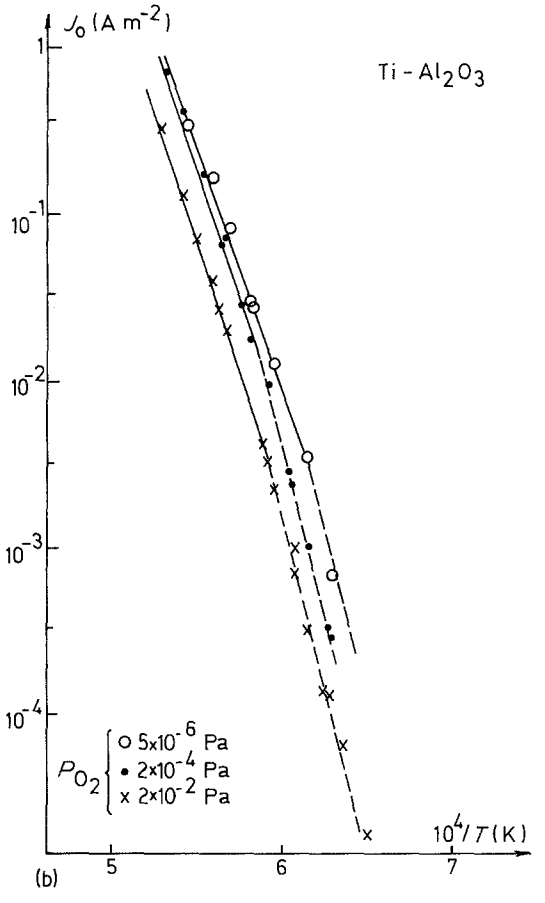

Figure 5 (a) Electron emission of polycrystalline Ti-doped Al_2O_3 as a function of temperature: the activation energy is $5.5 \leqslant E_{act} \leqslant 5.9$ eV. (b) Electron emission of polycrystalline Ti-doped Al_2O_3 as a function of P_{O_2}.

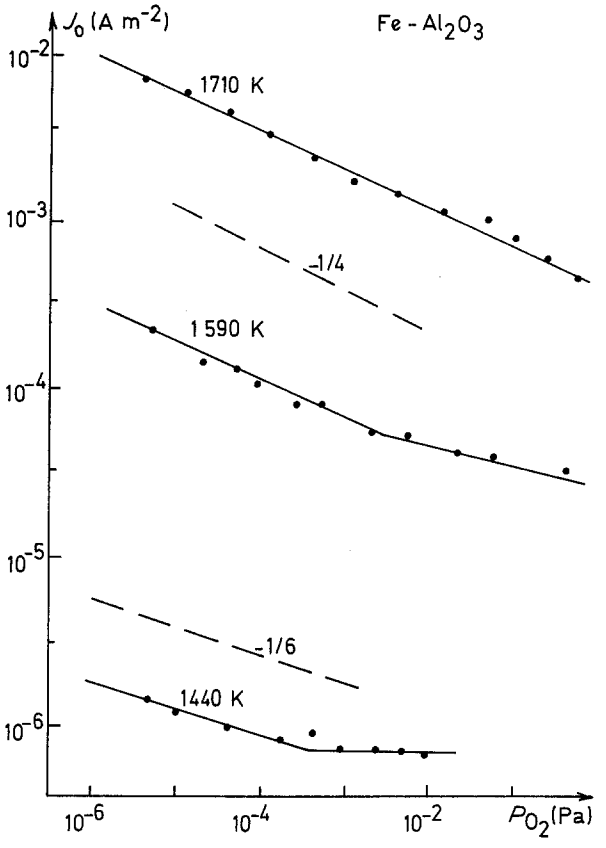

Figure 6 Electron emission of polycrystalline Fe-doped Al_2O_3 as a function of P_{O_2}.

not well controlled and may have changed during the experiment made at high temperature by isothermal runs.

The isotherms of Fig. 5b, show a plateau at low P_{O_2}, followed by a decrease in the current at high oxygen partial pressure. The slope in a log–log plot is between $-1/3.8$ and $-1/3.6$.

4.3. Iron-doped alumina

The iron-doped alumina had an initial doping of 3 wt% iron and no spectrographic analysis was made. The sample was found to be dark yellow after the experiment which indicates that some iron remains in the sample. The results of isothermal experiments made as before for the titanium-doped samples are shown in Fig. 6a. The emission decreases with oxygen partial pressure with a slope, in a log–log plot, which is $-1/4$ at high temperature and $-1/6$ at low temperature. In this latter range the curve was significantly flatter at high P_{O_2}, defining a plateau as observed previously in titanium-doped Al_2O_3, but in the high oxygen pressure range. The activation energy of the emission in the low P_{O_2} range is nearly 6.6 eV, not far from the value for the technical alumina and for titanium-doped alumina.

5. Discussion

The discussion of the results reported above can be divided in two parts. The first is supported by a quantitative analysis of the data in terms of the work function. The importance of segregation of impurities on the value of the work function is emphasized. The second part accounts for the oxygen dependency of the emission results assuming it to be due to changes in the defect chemistry of the layer involved by the electron emission.

5.1. The Fermi level in aluminas at high temperature

From the results shown above (Figs. 4 to 6) and Equation 1 it is possible to calculate the work function Φ (Fig. 7). The work function so calculated is generally called the "effective work function" as opposed to the "Richardson work function" obtained from the energy of activation of the emission, the slope of plots of

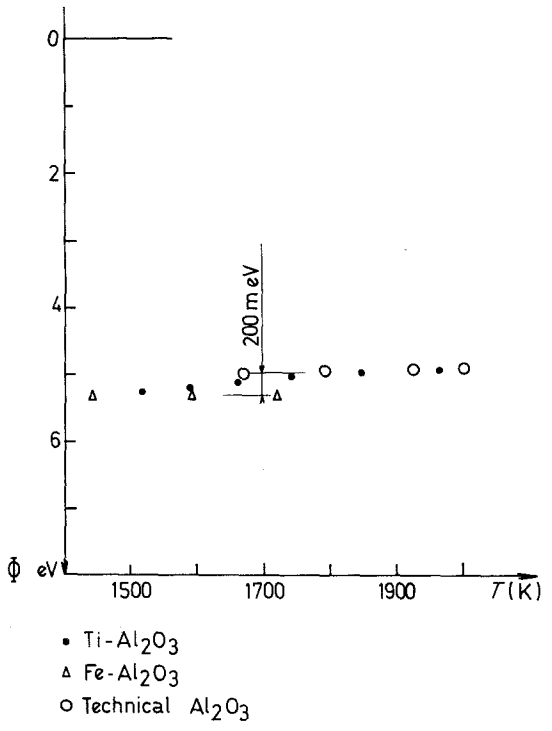

Figure 7 Dependence of Fermi level on temperature for several aluminas at $P_{O_2} = 2 \times 10^{-2}$ Pa calculated from the experimental results of Figs. 3 to 5. Also represented are the levels for Ti and Fe from [10].

$\log J_0/T^2 - 1/T$. The Richardson work function is equal to the work function at zero Kelvin and does not contain any information on the temperature dependence of Φ. On the other hand, as seen in Fig. 7, Φ changes weakly with T; the variation of Φ with T depending of the type of the impurity (for a general discussion see [23] or [35] in the more specific case of MgO). In a doped material with a compensated donor the work function Φ passes through a minimum as the temperature rises, the minimum corresponding to the exhaustion temperature. This temperature is shifted to lower temperature by addition of a compensating impurity. On this basis and from Fig. 7 it appears that the titanium-doped material is less compensated than the technical and iron-doped aluminas investigated here; this is in agreement with the chemical analysis.

From Fig. 7, the work function in aluminas ranges from 5.2 to 4.8 eV between 1500 and 1900 K, with a remarkable insensitivity to the doping by aliovalent impurities. Assuming a Fermi level pinned at the energy level of the impurity and from the position of the impurity levels given in Table II and Fig. 2, the Fermi level of titanium-doped Al_2O_3 should be approximately 3 eV below the conduction band and 4 to 5 eV for the iron-doped Al_2O_3: the work function should thus be different by approximately 1 eV for these two compounds. Two possibilities can be put forward to explain the observed behaviour:

1. the surface does not have the same composition as the bulk and does not follow the doping;

2. the surface is not very different from the bulk which is not completely doped, the doping level being insufficient to pass over the native impurities concentration.

This second hypothesis will be examined in Section 5.2.

The first case is discussed primarily and appears to be a consequence of segregation which is a very general process [36, 37], it is commonly interpreted in terms of one or other of two models. First, the surface and grain boundary of an ionic solid in equilibrium can carry an electrical potential resulting from the presence of an excess of ions of one sign [38], this is the case if the free energy of formation of anion and cation point defects differs [39]. The charge developed at the boundary is compensated by a space charge of the opposite sign. If aliovalent foreign atoms are present, they affect the concentration of native defects and take part in their redistribution. The second model is based on strain energy effects induced by differences between the ionic radii of the host and additive ions. In either case, especially with aliovalent impurities, the local neutrality of the crystal is not conserved and a space charge is created in the subgrain to compensate the boundary charge. Several hypotheses can be made concerning the repartition of the potential as a function of distance from the surface [38], in the frame of the double layer theory [40], the potential decreases exponentially with the distance x from the surface. Depending on the sign of the charges, the defect concentration is different in the bulk and in the subgrain. For example, if positive surface states exists, a negative space charge develops in the subgrain that repels positive charges to the bulk and accumulates negative charges near the surface. Thus the Fermi level will be closer to the bottom of the conduction band and the work function smaller (see Fig. 8a). An enrichment of subgrain in an impurity present in titanium-, iron-doped and technical alumina can explain why the work function is insensitive to the

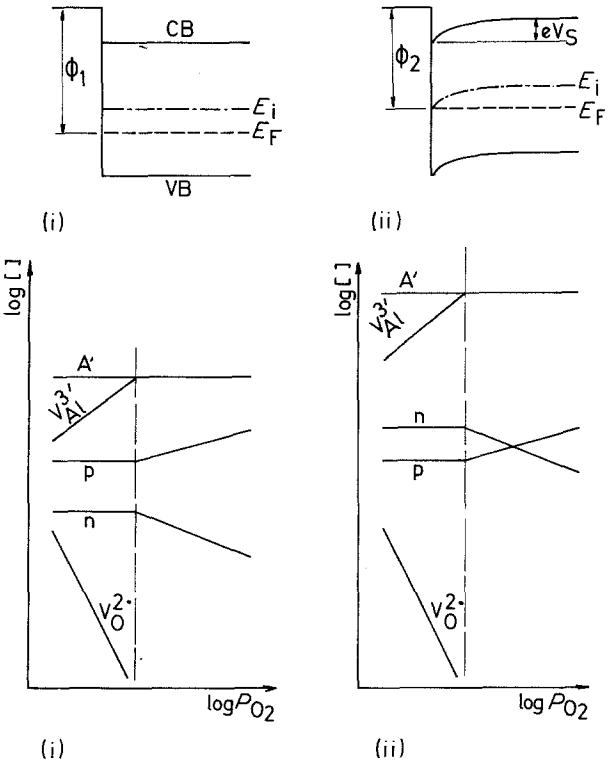

Figure 8 (a) Energy diagram versus the distance to the surface. Effect of segregation. (i) The surface has a composition identical with the bulk; (ii) the surface is enriched with positively charged atoms: the work function $\Phi_2 < \Phi_1$. (b) Plot of defect concentration against P_{O_2} in the bulk and in a boundary layer. (i) In the bulk; (ii) near the boundary, if positive charges are on the surface.

doping. Technical alumina probably behaves like an acceptor-dominated compound [8] as the iron-doped alumina does, in these materials the Fermi level is smaller (1 eV) than expected, it is thus possible that negatively charged atoms which are in excess in the acceptor-dominated materials are accumulated below the surface. Let us add that our titanium-doped compound also contains acceptor-type impurities (see Table III), eventually segregating and contributing to hide the bulk variations of the Fermi level.

This discussion underlines the real need to develop chemical characterization techniques of the surface and of the bulk operating at high temperature.

5.2. Effect of oxygen on emission: defect chemistry

In the previous discussion the oxygen dependence of electron emission was not taken into account; it is the subject of the present section to discuss this and to emphasize the role of point defects. In several oxides (see, for example, [12–14]) it has been observed that the emission density changes with the oxygen partial pressure according to the defect chemistry of the particular oxide. In the absence of surface states (or energy band bending), the density of emitted electrons is proportional to the conducting electron concentration (bulk concentration) as can be shown simply by the application of the Fermi–Dirac statistics to Equation 1:

$$J_0 = A_0 T^2 \frac{n}{N_c} \exp -\frac{\chi}{kT} \qquad (4)$$

The number of conducting electrons, n, is related to P_{O_2} through the equilibria given in Table I. If segregation occurs, then the concentration of defects near the surface is no longer an equilibrium concentration as it is in the bulk. On the other hand, if the potential is assumed to decrease exponentially with x, then the concentration of the various charged species can be approximated by:

$$\log\left(\frac{N_i}{N_i^0}\right) = \pm z_i e \frac{\psi_0}{kT} \exp -\frac{x}{x_D} \qquad (5)$$

where the negative sign has to be taken if positive surface states are associated with the boundary (positive sign for negative surface states). In Equation 5, ψ_0 is the potential at the boundary, $z_i e$ the charge on a species i, N_i the concentration at a distance x, N_i^0 the equilibrium concentration of i in the bulk and $1/x_D$ the double layer thickness or the Debye length. From Equation 5 it follows that the defect concentration depends on

x but remains proportional to the bulk value and thus keeps the same dependence on P_{O_2} [41] (see Fig. 8b). Accordingly, the emission density should have the same variations with P_{O_2} as the electron bulk concentration. In that respect the electrical conductivity is more complicated, because it involves both negative and positive charge carriers. The conductivity may thus have an n-type characteristic in the boundary layer while it is p-type in the bulk if negative charges accumulate below the surface.

The case of a technical alumina is considered first with the aim of discussing the absence of emission variation with P_{O_2} (Fig. 4a). As the electron concentration involved in the emission is expected to be proportional to that of the bulk, we will calculate that contribution in the bulk. The technical alumina has a relatively low purity (99.7%) and impurities should thus play an important role. Donor impurities are sodium, titanium, zirconium . . . , 400 ppm and acceptor impurities of magnesium, iron, nickel, zinc, cobalt . . . , 2700 ppm. Acceptor impurities are in the majority, but due to the presence of donors, the Fermi level is raised toward the centrum of the band gap; the acceptor levels are thus highly ionized. The absence of variation of n with P_{O_2} seen in Fig. 4a shows that electrons are not created by intrinsic non-stoichiometric defects: $V_O^{2\cdot}$, $Al_i^{3\cdot}$, $V_{Al}^{3\prime}$, but more likely by ionization of an impurity level. If acceptor levels are ionized, in order to explain a variation of n with T readily observed (see Fig. 4b), we have to suppose that a donor level is not completely ionized, owing to its deep position in the band gap. Considering Fig. 2, this hypothesis is plausible. The electroneutrality is thus written:

$$[\Delta\cdot] + [D\cdot] = [A'] \qquad (6)$$

where $[\Delta\cdot]$ are un-ionized donors whose concentration is related to n by $n[\Delta\cdot]/[\Delta^x] = k_\Delta$. $[D\cdot]$ is the concentration of all the ionized donors and $[A']$ the acceptors. It has been seen for another sample of technical alumina [27], that the emission decreases with P_{O_2} above 10^{-3} Pa (at 1700 K). This is proof that in that case $V_{Al}^{3\prime}$ are present, instead of $V_O^{2\cdot}$ or $Al_i^{3\cdot}$ that would induce an oxygen dependency at low P_{O_2}. Equation 6 has to be modified to take account of the $V_{Al}^{3\prime}$ in the high P_{O_2} range:

$$[\Delta\cdot] + [D\cdot] = [A'] + 3[V_{Al}^{3\prime}] \qquad (7)$$

In the range where Equation 6 is valid, e.g. at low P_{O_2}, the electron concentration is

$$n = k_\Delta \frac{([\Delta_{tot}] - [A'] + [D\cdot])}{[A'] - [D\cdot]} \qquad (8)$$

The oxygen pressure where $V_{Al}^{3\prime}$ becomes competitive in Equation 7 depends very much on $[A'] - [D\cdot]$. A small rise in $[D\cdot]$ has a large effect on n and on the oxygen pressure where $[V_{Al}^{3\prime}] > [A']$ (thus when Equation (7) can be approximated by $3[V_{Al}^{3\prime}] = [\Delta\cdot] + [D\cdot]$). In that new regime, when n decreases with P_{O_2}, such behaviour has been observed for titanium-doped alumina (see Fig. 5b) which show an emission independent of P_{O_2} but a decrease with increasing P_{O_2} above 10^{-5} Pa. Let us note that the emission of the plateau is slightly higher than for a technical alumina, as expected from Equation 8 if $[D\cdot]$ has risen. According to the defect chemistry (Table I), we should observe in that range $n \propto P_{O_2}^{-3/16}$ if $[\Delta\cdot] > [D\cdot]$ and $n \propto P_{O_2}^{-1/4}$ for the contrary. The slope of the experimental low is closer to $-1/4$ than to $-3/16$. Other possibilities such as interstitial oxygens ($[O_i'] = [\Delta\cdot] + [D\cdot]$) also give a law of $-1/4$. In fact, interstitial oxygen cannot be excluded in polycrystalline alumina: O_i^x is probably the major diffusing species at the grain boundaries [31]; O_i is also invoked to explain the features of dislocation near rutile precipitates in single crystal Al_2O_3 [42].

The behaviour of iron-doped Al_2O_3 (Fig. 6), is different from that of titanium-doped Al_2O_3: there is a decrease in emission at low oxygen pressure followed by a plateau at high P_{O_2}. At low P_{O_2}, the iron impurities favour the formation of $V_O^{2\cdot}$ or $Al_i^{3\cdot}$ [4] and give a dependence of the emission on P_{O_2}. The slope $-1/4$ is consistent with $V_O^{2\cdot}$ and ionized acceptors ($[Fe_{Al}'] = 2[V_O^{2\cdot}]$). At lower temperatures a smaller slope could be explained by a decrease in the ionization degree of the acceptor states. At high P_{O_2}, a compensation between donor impurities and iron-substituted atoms explains the plateau. From the relatively high position of the iron-level in the band gap of Al_2O_3 (Fig. 2), a partial ionization of that level can be assumed. The situation is, therefore, symmetrical to that described for the titanium-doped Al_2O_3.

From the above discussion it is seen that the absence of variation in the electron concentration with P_{O_2}, which was observed in these aluminas, is the consequence of an incomplete doping: impurities are in too high a concentration with respect

to the doping concentration. This, in turn, could explain why the absolute value of the emission is not very different from one sample to another.

6. Conclusion

Experiments made on various aluminas (technical, titanium- and iron-doped) have shown that the work function in these compounds is of the order of 5 eV at 1873 K. The Fermi level position, relative to the conduction band edge at the surface, is not very different from one sample to another. This fact indicates a possible segregation of a common species to these materials and a band curvature at the surface as a consequence.

It was found that a common feature of these compounds is to have a range where the electron concentration is independent of P_{O_2}. This was interpreted within the frame of point-defect theory as a consequence of self compensation between donor and acceptor impurities. In these samples, the doping concentration is not high enough to control the electronic properties of the layer.

Acknowledgements

The authors would like to thank Professor F. A. Kröger for originally suggesting the experiment and providing samples, and Dr A. M. Anthony and Dr M. Sayer for helpful discussions and corrections.

References

1. R. J. BROOK, J. YEE and F. A. KRÖGER, *J. Amer. Ceram. Soc.* **54** (1971) 444.
2. J. YEE and F. A. KRÖGER, *ibid.* **56** (1973) 189.
3. B. V. DUTT, J. P. HURREL and F. A. KRÖGER, *ibid.* **58** (1975) 420.
4. B. V. DUTT and F. A. KRÖGER, *ibid.* **58** (1975) 474.
5. S. K. MOHAPATRA and F. A. KRÖGER, *ibid.* **60** (1977) 141.
6. *Idem, ibid.* **60** (1977) 381.
7. *Idem, ibid.* **61** (1978) 106.
8. S. K. MOHAPATRA, S. K. TIKU and F. A. KRÖGER, *ibid.* **62** (1979) 50.
9. L. D. HOU, S. K. TIKU, H. A. WANG and F. A. KRÖGER, *J. Mater. Sci.* **14** (1979) 1877.
10. S. K. TIKU and F. A. KRÖGER, *J. Amer. Ceram. Soc.* **63** (1980) 31.
11. E. TANI and J. F. BAUMARD, *J. Solid State Chem.* **32** (1980) 105.
12. P. ODIER and J. P. LOUP, *ibid.* **34** (1980) 107.
13. J. C. RIFFLET, P. ODIER, A. M. ANTHONY and J. P. LOUP, *J. Amer. Ceram. Soc.* **58** (1975) 493.
14. P. ODIER and J. P. LOUP, "Advances in Ceramics", Vol. 3, Science and Technology of Zirconia (The American Ceramic Society, Columbus, 1981).
15. J. PAPPIS and W. D. KINGERY, *J. Amer. Ceram. Soc.* **44** (1961) 459.
16. J. P. LOUP and A. M. ANTHONY, *Rev. Int. Hautes Temp Refract.* **1** (1964) 15.
17. J. P. LOUP, N. JONKIERE and A. M. ANTHONY, *High Temp. High Press.* **2** (1970) 75.
18. O. T. OZKAN and A. J. MOULSON, *J. Phys. D: Appl. Phys.* **3** (1970) 983.
19. H. M. KIZILYALLI and P. R. MASON, *Phys. Status Solidi (a)* **36** (1976) 499.
20. K. KITAZAWA and R. L. COBLE, *J. Amer. Ceram. Soc.* **57** (1974) 246.
21. H. P. R. FREDERIKSE and W. R. HOSLER, "Material Science Research", Vol. 9, edited by A. R. Cooper (Plenum Press, New York, 1975).
22. F. A. KRÖGER, "The Chemistry of Imperfect Crystals" (North Holland, Amsterdam, 1974).
23. J. S. BLAKEMORE, "Semi-conductor Statistics", (Pergamon Press, Oxford, 1962).
24. C. KITTEL, "Introduction to Solid State Physics", 5th Edn. (Wiley, New York, 1976).
25. C. R. VISWANATHAN and R. Y. LOO, *Appl. Phys. Lett.* **21** (1972) 370.
26. Yu. I. SEMOV, *Phys. Status Solidi (a)* **32** (1969) K41.
27. P. ODIER and J. C. RIFFLET, *Int. J. Thermophysics* **2** (1981) 187.
28. B. BENDER, D. B. WILLIAMS and M. R. NOTIS, *J. Amer. Ceram. Soc.* **63** (1980) 542.
29. W. C. JOHNSON and D. F. STEIN, *J. Amer. Ceram. Soc.* **58** (1975) 485.
30. S. K. TIKU and F. A. KRÖGER, *ibid.* **63** (1980) 183.
31. H. A. WANG and F. A. KRÖGER, *ibid.* **63** (1980) 613.
32. J. NOWOTNY and J. B. WAGNER, *Oxid. Metals* **15** (1981) 169.
33. M. P. HARMER and R. J. BROOK, *J. Mater. Sci.* **15** (1980) 3017.
34. M. M. EL-AIAT, L. D. HOU, S. K. TIKU, H. A. WANG and F. A. KRÖGER, *J. Amer. Ceram. Soc.* **64** (1981) 174.
35. J. R. STEVENSON and E. B. HENSLEY, *J. Appl. Phys.* **32** (1961) 166.
36. W. D. KINGERY, *J. Amer. Ceram. Soc.* **57** (1974) 1.
37. A. M. STONEHAM, *ibid.* **64** (1981) 54.
38. W. D. KINGERY, "Grain Boundary Phenomena in Electronic Ceramics", Advances in Ceramics Vol. 1, (The American Ceramic Society, Columbus, 1981) p. 1.
39. J. FRENKEL, "Kinetic Theory of Liquids" (Oxford University Press, New York, 1946) p. 37.
40. E. J. WERVEY and J. Th. G. OVERBEEK, "Theory of The Stability of Lyophobic Colloids" (Elsevier, Amsterdam, 1948).
41. D. W. READEY, "Grain Boundary Phenomena in Electronic Ceramics", Advances in Ceramics Vol. 1, (The American Ceramic Society, Columbus, 1981) p. 453.
42. D. S. PHILIPS, T. E. MITCHELL and A. H. HEUER, *Phil. Mag. A* **42** (1980) 417.
43. E. A. COLOBOURN and W. C. MACKRODT, *Solid State Commun.* **40** (1981) 265.

44. C. J. DELBECK, S. A. MARSHALL and P. H. YUSTER, *Phys. Status Solidi(b)* **99** (1980) 377.
45. D. S. McCLURE, *J. Chem. Phys.* **36** (1962) 2757.
46. C. F. BAUER and D. H. WHITMORE, *J. Sol. State Chem.* **11** (1974) 38.
47. H. H. TIPPINS, *Phys. Rev. B* **1** (1970) 126.
48. C. F. YEN and R. L. COBLE, *J. Amer. Ceram. Soc.* **62** (1979) 89.
49. J. B. BLUM, H. L. TULLER and R. L. COBLE, *ibid.* **65** (1982) 379.

Received 20 December 1982
and accepted 21 September 1983